Saturation effect of background temperature and aridity on vegetation phenological sensitivity to urban warming

Zhang Zhenzhen[1#], Hu Xinxin[1#], Zhang Yongqi[1], Cui Shufen[2], Sun Liheng[3], Lin Xingwen[1*], Wu Chaofan[1], Zhang Zhaoyang[1], Chen Yuanjian[1], Wen Qingqing[4]

[1]College of Geography and Environmental Sciences, Zhejiang Normal University, Jinhua 321004, China

[2]College of Business, Lishui University, Lishui 323200, China

[3]Faculty of Management, Universiti Teknologi Malaysia, Johor Bahru 81310, Malaysia

[4]The Administration Center of Jinhua Wucheng Nanshan Provincial Nature Reserve, Jinhua 321000, China

*** Correspondence: Lin Xingwen (linxw@zjnu.edu.cn)**

[#] **These authors contributed equally to this work**

Abstract:

Quantifying how background temperature and aridity constrain phenological sensitivity to urban warming requires identifying critical thermal thresholds and hydrological boundaries driving spatial heterogeneity. This study assessed urban warming effects on vegetation phenology across 293 Chinese cities during 2010–2020. Urban-rural disparities (ΔSOS, ΔEOS) and temperature sensitivity ($R_{t\text{-}SOS}$, $R_{t\text{-}EOS}$) were quantified using satellite metrics. Results showed that urban heat islands advanced SOS by 12.06 days and delayed EOS by 9.86 days relative to rural areas. A non-linear saturation effect was detected: phenological sensitivity to urban warming peaked at 4 ℃ (spring) and 6 ℃ (autumn), and significantly weakened beyond sensitivity saturation thresholds of 12.5 ℃ (SOS) and 4 ℃ (EOS). Aridity acted as a

negative regulator that weakened warming benefits across most aridity index (AI) ranges and reversed them within 1.4 < AI < 2.0. Combined, LST and AI explained 75.05% and 76.21% of spatial variance in SOS and EOS responses, respectively. Conceptually, these findings challenge the linear paradigm of warming-driven phenological shifts by demonstrating finite physiological benefits of urban warming. Ecologically, this study highlights the coupled heat-aridity constraints on urban vegetation, providing key implications for climate-adaptive urban ecological planning.

Keywords: urbanization; heat island effect; vegetation phenological sensitivity; aridity index; land surface temperature; saturation effect

1. Introduction

Vegetation phenology, a critical aspect of ecosystem dynamics, exhibits significant sensitivity to the coupling of thermal and moisture variations (Badeck et al., 2004; Yu et al., 2003). While recent studies have shown that urban warming advances the start of the growing season (SOS) and delays the end of the growing season (EOS), it is increasingly recognized that these responses are not solely temperature-driven but are fundamentally constrained by the background aridity of the locale. Thus, the phenological "benefits" of the Urban Heat Island (UHI) effect must be evaluated through a dual lens of heat and water availability (Jeong et al., 2019). The cascading effects of these shifts extend beyond mere phenological alterations, contributing to a range of ecological and environmental challenges (Zhou et al., 2016; Qiu et al., 2017; Ding et al., 2020).

However, the degree to which warming benefits phenological changes has been widely debated (Chmielewski and Rötzer, 2001; Ding et al., 2020; Yao et al., 2017). Urban environments offer a unique "natural laboratory" for testing these phenological theories. Unlike experimental warming plots, the urban heat island (UHI) effect represents a sustained, large-scale warming scenario that has persisted for decades (Grimm et al., 2008). This allows researchers to observe long-term vegetation adaptation and identify thresholds that are difficult to capture in short-term

manipulative experiments. Moreover, the vast geographic distribution of cities across climatic gradients provides a natural experimental framework to test how identical warming magnitudes (UHI) interact with varying background climates (Fig. 1). Empirical evidence from the Northern Hemisphere consistently shows that cities in cold high-latitude regions exhibit more advanced SOS and delayed EOS in response to urban warming (Dallimer et al., 2016; Gazal et al., 2008; Jia et al., 2021; Li et al., 2021; Meng et al., 2020). While these studies offer valuable evidence regarding spatial heterogeneity, the non-linear dynamics of these responses—specifically, the saturation thresholds where urban warming benefits diminish, and how background aridity modulates these thresholds—remain inadequately quantified across climatic gradients. Identifying such thresholds is critical for predicting urban ecosystem stability under continuous global warming scenarios.

The magnitude of urban-induced phenological shifts is not uniform. Background climate heterogeneity constrains vegetation responses to additional urban warming: phenological advancements are strong in cold regions but weaken as baseline temperatures rise, implying that phenological sensitivity is a variable state conditioned by local thermal conditions. In ecology, the "saturation effect" describes that stimulus efficacy declines beyond a threshold, rooted in tolerance curve theory (Angilletta, 2009): organismal physiological functions increase with environmental drivers until reaching physiological saturation, beyond which no further enhancement occurs (Ketola and Kristensen, 2017). Plant physiological processes (photosynthesis, respiration, transpiration) do not increase linearly with temperature; they slow down or even decrease beyond a thermal threshold (Sage and Kubien, 2007; Ge et al., 2021). Meta-analysis has shown greater positive growth responses to warming in colder ecosystems (Rustad et al., 2001; Büntgen et al., 2019). We therefore hypothesize that urban warming benefits for phenology (advanced SOS, delayed EOS) gradually approach saturation in warmer regions, and extra UHI warming will no longer promote phenological shifts. This hypothesis remains to be tested in urban ecosystems.

Drought disrupts temperature-driven phenological responses (Peng et al., 2019;

Yuan et al., 2020). Urban vegetation is particularly vulnerable to moisture deficits due to the "Urban Dry Island" effect (reduced soil moisture and elevated evaporation in built environments) and impervious surfaces (Zhang et al., 2019). UHI warming combined with high aridity elevates vapor pressure deficit and water demand, triggering defensive mechanisms (such as ABA accumulation and protein degradation) (Brodribb and McAdam, 2013) that offset thermal advancements. Drought delays spring SOS and advances autumn EOS by inducing water stress and early dormancy (Brodribb and McAdam, 2013; Čehulić et al., 2019). However, in urban environments, this drought effect is compounded by the Urban Dry Island and impervious surfaces, further attenuating phenological sensitivity to extra warming, diminishing the positive impacts of UHI; this effect is stronger in warmer cities where plants approach thermal limits.

Consequently, we hypothesize that background aridity (AI) acts as a critical negative regulator of the thermal saturation threshold. Specifically, we predict that as background aridity increases, the "saturation point" at which warming benefits (such as advanced SOS or delayed EOS) plateau will occur at lower LST values. This implies that the saturation effect is not a fixed thermal threshold but a dynamic state conditioned by water stress, leading to a more rapid decline in phenological sensitivity in arid urban environments.

Furthermore, phenological sensitivity to environmental drivers is species-specific and modulated by functional traits. Broad-leaf and coniferous species show divergent responses to warming and drought due to differences in leaf morphology and hydraulic architecture (Zheng et al., 2022). However, whether the saturation effect and "aridity-driven inhibition" are consistent across urban vegetation types remains unclear.

As a rapidly urbanizing country with diverse climates, China faces severe UHI challenges (He et al., 2017). UHI intensity averages 0.9 ± 1.1 ℃ but varies drastically across regions (Li et al., 2021). Previous urban phenology studies focused on linear temperature sensitivity, ignoring non-linear saturation effects and aridity interactions. No study has quantified critical thermal/arid saturation thresholds or clarified the

coupling mechanism between pre-season temperature (T, phenological sensitivity) and land surface temperature (LST, background climate) in urban ecosystems. China's large climatic gradients and rapid urbanization make it an ideal platform to test the saturation hypothesis and aridity modulation.

Thus, an investigation into the phenological response of plants to urbanization in China would enhance our understanding of their ability to acclimate to climate change across various environments. However, how background temperature and aridity interact to determine the thresholds and "saturation" of phenological sensitivity to urban warming remains largely unquantified at the macro-scale. Addressing this gap is essential for predicting the stability of urban carbon sinks under future climate scenarios. To this end, the primary objectives of this study were to: (1) explore the spatial distribution of plant phenological responses to the urban heat island effect throughout mainland China; (2) quantify the saturation effect caused by the spatial variability of phenological responses correlated with background temperature across the cold-hot gradient; and (3) assess whether the benefits of urban warming would be counteracted in drought-affected areas.

2. Materials and Methods

2.1 Study area

In our study, we conducted an analysis covering a total of 293 prefecture-level cities in China (excluding Taiwan, Autonomous Prefecture, and regions), taking into account the data from the year 2020 (http://xzqh.mca.gov.cn/map) (Fig. 1). It was hypothesized that the urban warming effect is most pronounced in urban centers and gradually diminishes towards rural areas (Zhang et al., 2004). To determine the urbanization intensity of each city, nighttime light data from NPP-VIIRS (Table 1) were utilized (Elvidge et al., 2017), employing the reference comparison method. The optimal segmentation threshold was established based on the statistical yearbook (Fan et al., 2019). Moreover, urban built-up areas were identified using the comparison method and annual average data derived from NPP-VIIRS night lights between 2013 and 2020. All data processing procedures were performed using ArcGIS 10.2. We

created ten buffer zones extending to a radius of 20 km from each city center, with each zone representing a 2 km annulus (Fig. 1).

This 20 km boundary was chosen because our preliminary analysis revealed that the urban warming footprint on phenological metrics (SOS and EOS) gradually diminishes to near zero beyond 15 km (Zhang et al., 2004; Figs. 1 and 2). Thus, defining the outermost 20 km buffer zone as the "Rural" baseline guarantees a background environment conservatively free from urban heat island interference. The subscript (10) refers to the 10th buffer zone at 20 km from the urban center. Equation notations use a standardized buffer index (0 for urban center, 10 for rural reference) to avoid confusion between distance and buffer number.

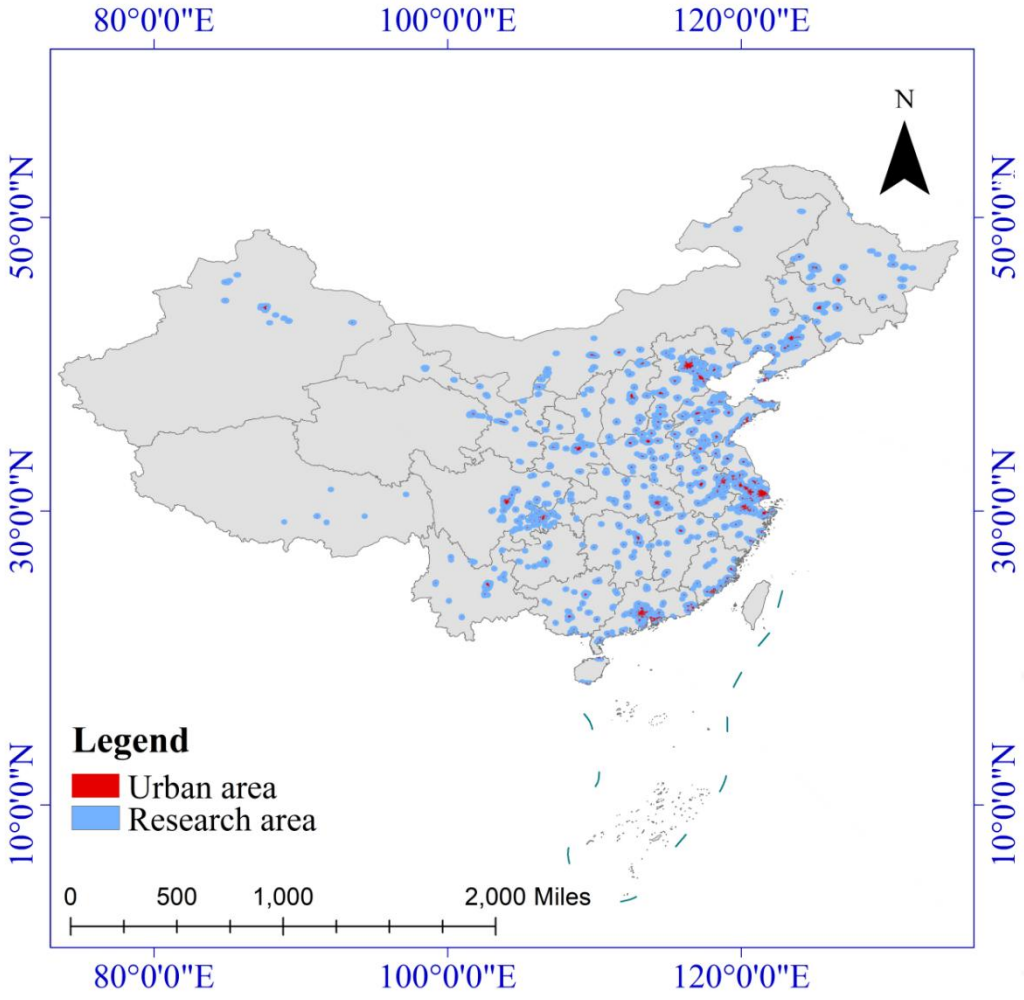

Figure 1. City centers (red area) and buffer zones (blue area) of the 293 prefecture-level cities in China. The map, generated using ArcGIS version 10.2 (https://www.esri.com/about/newsroom/arcwatch/the-best-of-arcgis-10-2/), features

administrative boundaries sourced from the Ministry of Civil Affairs of the People's Republic of China (http://xzqh.mca.gov.cn/map). Source: Esri, TomTom, FAO, USGS, and the GIS User Community; Ministry of Civil Affairs of the People's Republic of China | Powered by Esri.

2.2 Vegetation phenology extraction

Phenology data spanning the years 2010 to 2020 were derived from MODIS Enhanced Vegetation Index (EVI) 16-day composite data with a spatial resolution of 250 m (MOD13Q1) and processed with TIMESAT (Jönsson and Eklundh, 2004). To mitigate challenges such as cloud cover and snow, the raw EVI time series data were smoothed using the Savitzky-Golay (S-G) filter method (Cai et al., 2017). Subsequently, a dynamic threshold technique was employed to extract the phenology data, utilizing a seasonal amplitude of 20%, a parameter proven effective for phenology extraction in urban environments (Zhou et al., 2016; Buyantuyev and Wu, 2012; Cong et al., 2012; White et al., 2009). The datasets underwent preprocessing and quality control to eliminate pixels with minimal vegetation EVI (e.g., bodies of water and fully paved surfaces). To exclude unrealistic phenological values, we retained only SOS (30–180 days) and EOS (210–360 days) within valid ranges, consistent with previous studies (Zhang et al., 2006). Efforts were made to reduce the impact of outlier years by averaging the phenology data for each pixel across the timeframe from 2010 to 2020. After applying these quality control thresholds and land-cover filtering criteria, approximately 48.5% of the initial pixels within the study buffer zones were excluded.

Furthermore, we employed land cover data from the MCD12Q1 dataset, which has a 500-meter resolution, to mitigate the impact of agricultural practices on the mainland during our analysis. The MCD12Q1 dataset categorizes land into 17 distinct classes. These include various types of forested areas such as Evergreen Coniferous Forests, Deciduous Needle-leaf Forests, Evergreen Broad-leaf Forests, Deciduous Broad-leaf Forests, Mixed Forests, as well as Closed Shrub lands, Open Shrub lands, Savannas, Woody Savannas, Grasslands, and Croplands.

Given the frequent human-induced disturbances in rural croplands and the regular manual pruning of urban grasslands, we excluded savannas, woody savannas, grasslands, and croplands from our analysis. The remaining land types were consolidated into broader categories: broad-leaf forests (BF, deciduous and evergreen broadleaf forests), coniferous forests (CF, deciduous and evergreen coniferous forests), mixed forests (MF), and shrubs (closed and open shrublands). This classification approach allowed us to focus our analysis on land types that are less influenced by human activities.

Table 1. Data inventory used in this study

Data type	Resolution	Layer	Data sources	Year
MOD13Q1	250m/16d	EVI	https://search.earthdata.nasa.gov	2010-2020
MOD11A2	1000m/8d	LST_Day LST_Night	https://search.earthdata.nasa.gov	2010-2020
MOD16A2	500m/8d	PET	https://search.earthdata.nasa.gov	2010-2020
MCD12Q1	500m	Land Cover	https://search.earthdata.nasa.gov	2010-2020
VIIRS	500m	yearly average	https://eogdata.mines.edu	2013-2020
Precipitation data	1000m	monthly average	http://www.geodata.cn	2010-2020
China's urban zoning data			https://www.resdc.cn	2020
Station climates		monthly average	http://data.cma.cn/en	2010-2020

2.3 Pre-season temperature and background climates

Building upon the methodology of a previous study (Piao et al., 2006), we defined pre-season temperature (T) as the mean temperature for the three months preceding phenological onset. For alignment with the phenology information, the average temperature dataset was resampled to a 250 m resolution using the nearest neighbor interpolation technique. To evaluate the performance of the downscaling procedure, the observed long-term monthly temperature and precipitation across China were obtained from the National Meteorological Information Center of China (http://data.cma.cn/en). This dataset included observations from 496 national weather

stations during 2010 to 2020. Upon conducting a fitting analysis with station data, we observed that the coefficient of determination (R^2) for monthly mean temperature and remote sensing data reached 0.93, while that for monthly precipitation and remote sensing data achieved 0.85. These results indicated that the downscaled meteorological data sufficiently met the requirements of this study.

The background climates were evaluated utilizing land surface temperature (LST) and the aridity index (AI) as indicators. The LST and AI data for each pixel were averaged over 2010 to 2020. Specifically, MODIS LST datasets exhibiting an absolute bias of less than 1 K were selected as optimal for our investigation, in line with previous studies (Gow et al., 2016; Pablos et al., 2016; Qiao et al., 2013; Wan, 2008). Collection 6 LST products from the Aqua satellite (MOD11A2, 8-day composite, 1 km spatial resolution, covering the period from 2010 to 2020) were used. Additionally, daily temperature (T) was calculated as the mean of daytime and nighttime temperatures, following the methodology outlined by Kang et al. (2016). AI was expressed as:

$$AI = PET/P \quad (1)$$

where PET denotes the annual potential evapotranspiration and P denotes the annual precipitation. The PET values spanning from 2010 to 2020 were extracted from the MOD16A2 monthly synthetic product, characterized by an 8-day temporal resolution and a spatial resolution of 500 m (Mu et al., 2011), as delineated in Table 1. The annual precipitation (P) dataset was derived from the monthly precipitation records of China encompassing the timeframe from 1901 to 2020, at a spatial resolution of 1 km. Subsequently, both PET and P datasets were resampled to a spatial resolution of 250 m to facilitate the ensuing spatial analysis (Peng, 2020).

To robustly quantify these responses, we defined the distinct analytical roles of two critical thermal dimensions: pre-season air temperature (T) and land surface temperature (LST). In this study, T and LST serve strictly distinct analytical roles. As the direct biological driver of plant physiology (e.g., chilling requirements), T was used exclusively to quantify the pure biological phenological sensitivity (R_t) and identify true physiological thresholds. In contrast, as the standard metric for

quantifying the urban heat island (UHI) effect, LST was used to characterize the spatial "background climate" of each city across the continent.

Because pre-season air temperature (T) is the direct driver of phenological sensitivity, we first derived the biological thresholds using T (Fig. 5). However, to address our core objective of quantifying how background LST shapes these phenological shifts, we defined the quantitative relationship between the background LST and T. We fitted the relationship curve between LST and T across all cities. To minimize data matching biases during this conversion, we used the spatiotemporally aligned 10-year climatological means (2010–2020) for both variables at a unified 250 m resolution. We observed a highly robust linear correlation (Fig. S4). Based on this high goodness-of-fit, we applied the empirical conversion formula between the two variables to mathematically substitute T with LST in the sensitivity curves (Wan, 2008). This empirical translation allowed us to systematically convert the T-driven physiological thresholds into the specific LST-determined background climate thresholds (12.5 ℃ for SOS and 4 ℃ for EOS), explicitly projecting pure biological limits onto the urban map. Although T and LST represent different physical properties, they are highly correlated in urban settings ($R^2 = 0.93$ for monthly mean temperature), confirming the reliability of this empirical conversion between physiological response and climatic background.

2.4 Urbanization effect on phenology

The phenology dates of each vegetation type were extracted in each buffer zone. Finally, the mean phenology in each buffer zone was calculated as a weighted mean of the phenology of each vegetation type. To ensure comparability in phenological analyses across buffer zones, we first identified the common vegetation types present in all zones and excluded the non-shared types. We then calculated the phenological means for these common types within each buffer zone and averaged these values to determine the overall mean vegetation phenology for the entire buffer region, as shown in Eqs. (2) and (3).

$$SOS_i = \sum SOS_{ij} \Big/ n \tag{2}$$

$$EOS_i = \sum EOS_{ij} \Big/ n \quad (3)$$

263 SOS_i and EOS_i are the mean SOS and EOS of the i-th buffer zone; SOS_{ij} and EOS_{ij} are
264 the mean SOS and EOS of the j-th vegetation type in the i-th buffer zone; n is the
265 number of shared vegetation types across all buffer zones.

266 To investigate the impact of urbanization on phenology, mean values of start of
267 season (SOS) and end of season (EOS) in each buffer zone were analyzed during
268 2010–2020, and fitted with respect to their distance from the urban center. In this
269 study, the outermost buffer zone (20 km from the urban center) was defined as the
270 rural reference region, and the urban center was defined as the urban region. This
271 delineation was justified by the observation that phenological change rates
272 approached zero at 15 km and beyond (Fig. S1), and similar patterns were observed
273 for all four vegetation types (Fig. S2). Following prior investigations, the
274 phenological sensitivity (R_t) to temperature was quantified by calculating the partial
275 correlation coefficient between T and the phenology dates ($R_{t\text{-}SOS}$ and $R_{t\text{-}EOS}$) (Meng et
276 al., 2020). The phenological difference between urban and rural regions was
277 calculated to quantify the magnitude of the urban warming effect on phenology:

$$\Delta SOS = SOS_{(0)} - SOS_{(10)} \quad (4)$$

$$\Delta EOS = EOS_{(0)} - EOS_{(10)} \quad (5)$$

278 where $SOS_{(0)}$ and $SOS_{(10)}$ are the mean SOS of the urban center (buffer index 0) and
279 the 10th buffer zone (located 20 km away), respectively. Similarly, $EOS_{(0)}$ and $EOS_{(10)}$
280 are the mean EOS of the urban center and the 10th buffer zone. Biologically, a
281 negative ΔSOS indicates an advanced start of the season (spring) in the urban center
282 relative to the rural area, while a positive ΔEOS indicates a delayed end of the season
283 (autumn senescence) in the urban center.

284 Similarly, the difference in phenological sensitivity to temperature between
285 urban and rural regions was defined as:

$$\Delta R_{t-SOS} = R_{t-SOS(0)} - R_{t-SOS(10)} \quad (6)$$

$$\Delta R_{t-EOS} = R_{t-EOS(0)} - R_{t-EOS(10)} \quad (7)$$

286 where $R_{t\text{-}SOS(0)}$ and $R_{t\text{-}SOS(10)}$ are the mean $R_{t\text{-}SOS}$ of the urban center (buffer index 0)

and the 10th buffer zone (located 20 km away), respectively. Similarly, $R_{t\text{-}EOS(0)}$ and $R_{t\text{-}EOS(10)}$ are the mean $R_{t\text{-}EOS}$ of the urban center and the 10th buffer zone.

2.5 Background climates determined phenology response

To elucidate the distinct impacts of LST and AI on urban and rural components, we performed a partial correlation analysis. Specifically, the average LST or AI values for 2010 to 2020 for each of the 293 cities were correlated with their respective ΔSOS, ΔEOS, $\Delta R_{t\text{-}SOS}$, and $\Delta R_{t\text{-}EOS}$ values, while we controlled for the influence of the other climatic factor.

Path analysis (PA) (Doncaster, 2007) was used to examine both the direct and indirect effects of background climate variables (LST and AI) on phenological responses (SOS and EOS), as well as their corresponding discrepancies (ΔSOS and ΔEOS) and rates of change ($\Delta R_{t\text{-}SOS}$ and $\Delta R_{t\text{-}EOS}$).

In the path analysis, we first assessed model fit using fit indices, including the chi-square (χ^2) statistic, Comparative Fit Index (CFI), and Root Mean Square Error of Approximation (RMSEA). Then, path coefficients were derived for both the direct and indirect effects of each independent variable on the dependent variable from the model. Squared path coefficients were used to estimate the respective direct and indirect contributions of each independent variable to the dependent variable. The sum of these direct and indirect contributions represents the total contribution degree, or relative contribution.

2.6 Validation of phenology "saturation effect"

To determine if there was a temperature saturation effect on vegetation phenology, we conducted a model comparison. Rather than assuming a single relationship a priori, we evaluated the fit of phenology versus pre-season temperature using competing models: a linear model, a quadratic model, a segmented (piecewise) model, and a logistic model. We specifically selected the logistic function as our primary model because quadratic models biologically imply a symmetric reversal (a continuous steep decline) rather than a plateau, and piecewise models assume an

abrupt, angular change in biological rates, which is less physiologically realistic than the smooth, asymptotic transition captured by the logistic curve (Pinheiro and Bates, 2000). The asymptote of the logistic function mathematically represents the biological "saturation point" — the maximum physiological limit of thermal benefits.

Statistically, the model comparison results (Table 2) confirm that the logistic model consistently outperforms the other three formulations for both spring SOS and autumn EOS, providing quantitative support for the non-linear saturation effect interpretation. For SOS, the logistic model yields an AIC value 2778 units lower than the linear model and 1424 units lower than the piecewise model, along with an R^2 of 0.37, which is approximately 19% higher than the second-best piecewise model. For EOS, the logistic model still achieves the lowest AIC and highest R^2, but the performance improvement is more modest: its R^2 (0.40) is only marginally higher than that of the piecewise model (0.39), consistent with a weaker but stable saturation pattern.

Table 2. Performance comparison of four competing models describing phenological responses to pre-season temperature

Phase	Model	AIC	BIC	R^2	RMSE
Spring_SOS	Linear	104203.62	104218.97	0.25	26.52
	Quadratic	103636.33	103659.35	0.27	26.05
	Piecewise	102849.67	102880.36	0.31	25.41
	Logistic	101425.33	101456.02	0.37	24.29
Autumn_EOS	Linear	93252.94	93268.34	0.23	17.39
	Quadratic	90241.5	90264.6	0.36	15.86
	Piecewise	89309.4	89340.2	0.39	15.41
	Logistic	85678.49	85709.14	0.40	15.22

We then extracted phenological information from all vegetation pixels across the country and generated scatter plots of phenology versus pre-season temperature. Next, we fitted logistic growth curves to these scatter plots and evaluated the assumption using the goodness-of-fit metrics, p-value and R^2. Subsequently, we applied the same

logistic curve to characterize the phenological responses of urban and suburban vegetation in 293 different cities against their pre-season temperatures, testing whether the phenological response to temperature in urban areas also follows a logistic growth pattern. Finally, we replaced the pre-season temperature with the background temperature LST to determine how the phenological saturation effect is regulated by the background temperature.

3. Results

3.1 Spatial distribution of urban-rural phenological differences

Among the 293 cities analyzed, 84% (N = 246) exhibited an advanced SOS in urban areas compared to rural regions, while 82% (N = 241) showed a delayed EOS (Fig. S3). Spatially, cities located in high-latitude regions generally demonstrated more negative ΔSOS values than those in low-latitude regions (Fig. 2), indicating that urban warming advanced spring phenology most strongly in northern and western China (Fig. 2a,b). This pattern is consistent with the conventional understanding of earlier SOS in colder regions. Additionally, cities in coastal provinces exhibited larger ΔSOS values than inland cities (Fig. 2).

A strong positive correlation was observed between ΔSOS and the rural rate of SOS change ($R_{t\text{-}SOS}$), suggesting that cities with more negative $R_{t\text{-}SOS}$ values exhibited larger urban-rural disparities (Fig. 3). Notably, cities with lower temperatures tended to have more negative $R_{t\text{-}SOS}$ and ΔSOS values.

ΔEOS also showed a significant increasing trend with latitude (Fig. 2), with northern cities displaying more positive ΔEOS values, indicating a delayed autumn phenology in urban areas (Fig. 2c,d). In contrast, the majority of cities in southern regions demonstrated negative ΔEOS values, signifying an advancement in autumn phenology. Furthermore, cities in the coastal provinces also exhibited larger ΔEOS values.

Similarly, a positive correlation was observed between ΔEOS and the rural rate of EOS change ($R_{t\text{-}EOS}$). Positive and negative ΔEOS values were predominantly found in cold and warm regions, respectively (Fig. 3). Moreover, when ΔEOS > 0,

both the absolute value of ΔEOS and $\Delta R_{t\text{-}EOS}$ increased with temperature, while for ΔEOS < 0, the absolute value of ΔEOS and $\Delta R_{t\text{-}EOS}$ decreased with temperature.

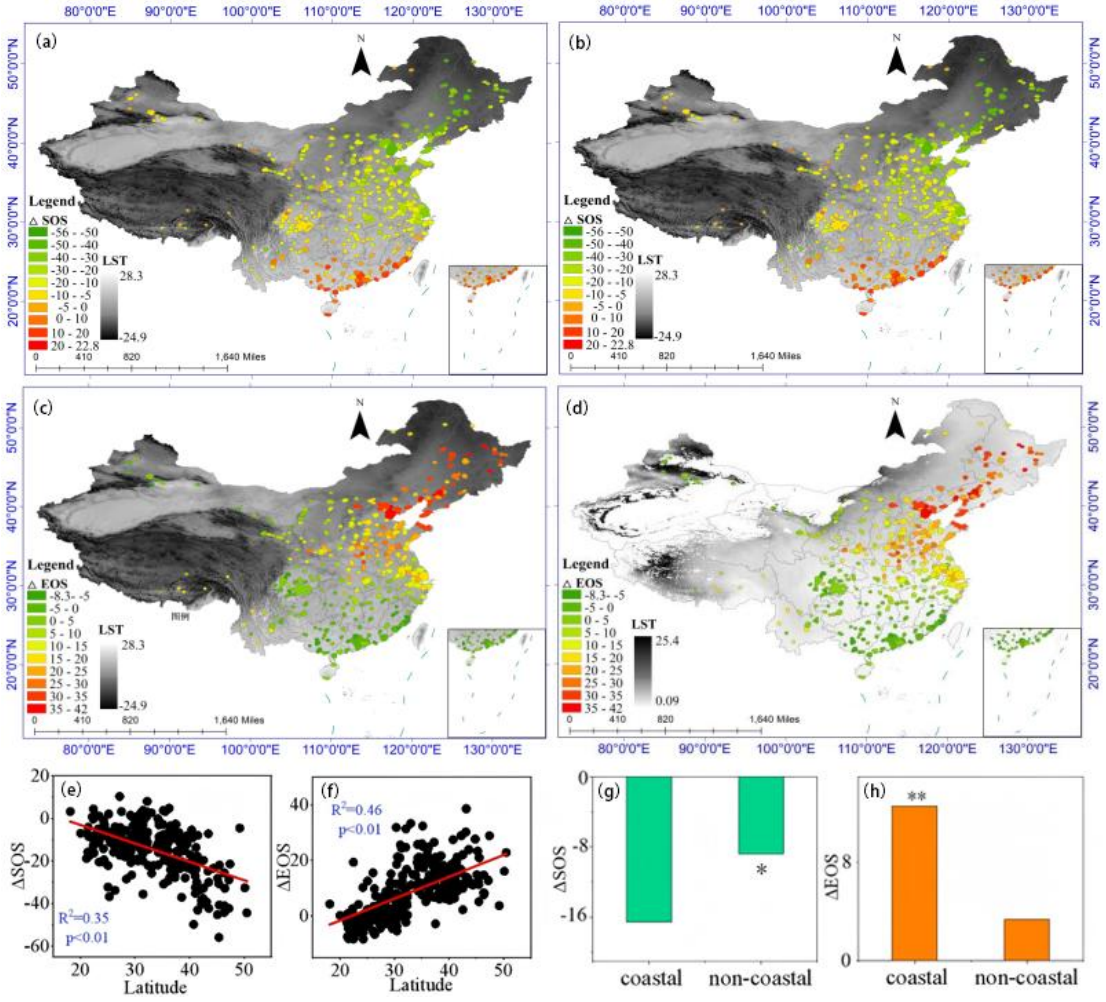

Figure 2. Spatial distributions of urban-rural disparities in SOS (ΔSOS) (a and b) and in EOS (ΔEOS) (c and d) across mainland China. Mean land surface temperature (LST) is shown in grayscale for the study area, and the data reflect the 10-year mean for 2010–2020 for each city.

Panel (e) depicts the linear correlation between ΔSOS and latitude ($R^2 = 0.35$, $p < 0.01$);

panel (f) depicts the linear correlation between ΔEOS and latitude ($R^2 = 0.46$, $p < 0.01$);

panel (g) compares ΔSOS between coastal and non-coastal provinces (*$p < 0.05$);

panel (h) compares ΔEOS between coastal and non-coastal provinces (**$p < 0.01$).

The map, generated using ArcGIS version 10.2, features administrative boundaries

sourced from the Ministry of Civil Affairs of the People's Republic of China (http://xzqh.mca.gov.cn/map). Source: Esri, TomTom, FAO, USGS, and the GIS User Community; Ministry of Civil Affairs of the People's Republic of China | Powered by Esri.

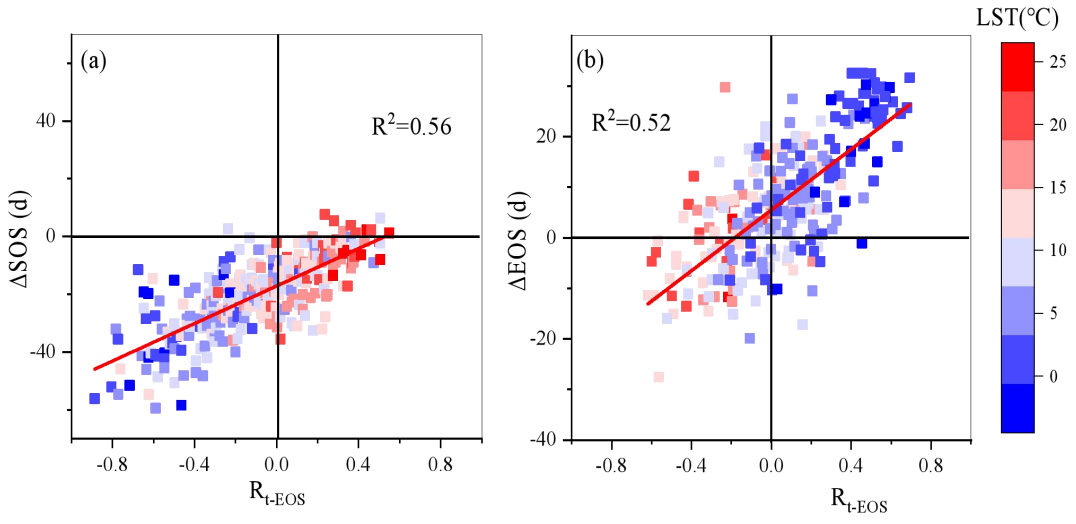

Figure 3. Relationship between urban-rural phenological difference and temperature sensitivity across 293 Chinese cities.

(a) Urban-rural difference in start of growing season (ΔSOS) versus temperature sensitivity of SOS ($R_{t\text{-}SOS}$).

(b) Urban-rural difference in end of growing season (ΔEOS) versus temperature sensitivity of EOS ($R_{t\text{-}EOS}$).

Each point represents one of the 293 cities analyzed, colored by land surface temperature (LST, ℃). Red solid lines indicate linear regression fits.

3.2 Phenology response to LST

As we compared urban and rural regions, logistic trends were observed for both SOS and EOS in relation to LST (Fig. 4). In urban areas where LST was below 12 ℃, the SOS occurred notably earlier compared to rural areas, while urban areas exhibited a delayed EOS when LST was below 18.5 ℃. As LST decreased, the SOS stabilized at 101.3 days for urban regions and 129.7 days for rural regions, while the EOS stabilized at 321.3 days for urban areas and 310.8 days for rural areas. In contrast,

when LST exceeded the specific thresholds for urban-rural differences (LST = 18 ℃ for ΔSOS and LST = 18.5 ℃ for ΔEOS), the phenological disparities between urban and rural areas were no longer significant and sometimes even reversed (Fig. 4a,b). As LST increased, the urban and rural SOS stabilized at 71.7 days (Fig. 4a), and the urban and rural EOS stabilized at 327.4 days and 332.4 days, respectively. Fitted curves of ΔSOS and ΔEOS with LST revealed positive and negative relationship, respectively, intersecting at LST = 18 ℃ and 18.5 ℃, indicating a shift in SOS and EOS dynamics with increasing temperatures beyond these thresholds.

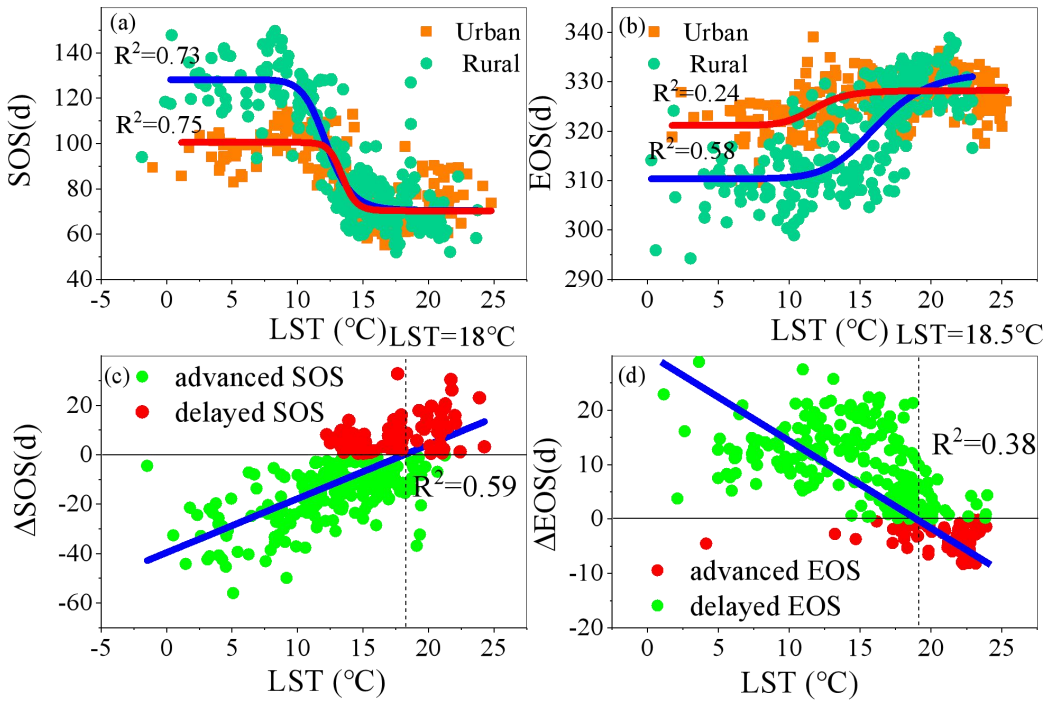

Figure 4. Relationship between background temperature (LST) and phenology (SOS and EOS) in urban and rural areas (a, b) for 2010 to 2020, and between ΔSOS and LST and between ΔEOS and LST (c,d).

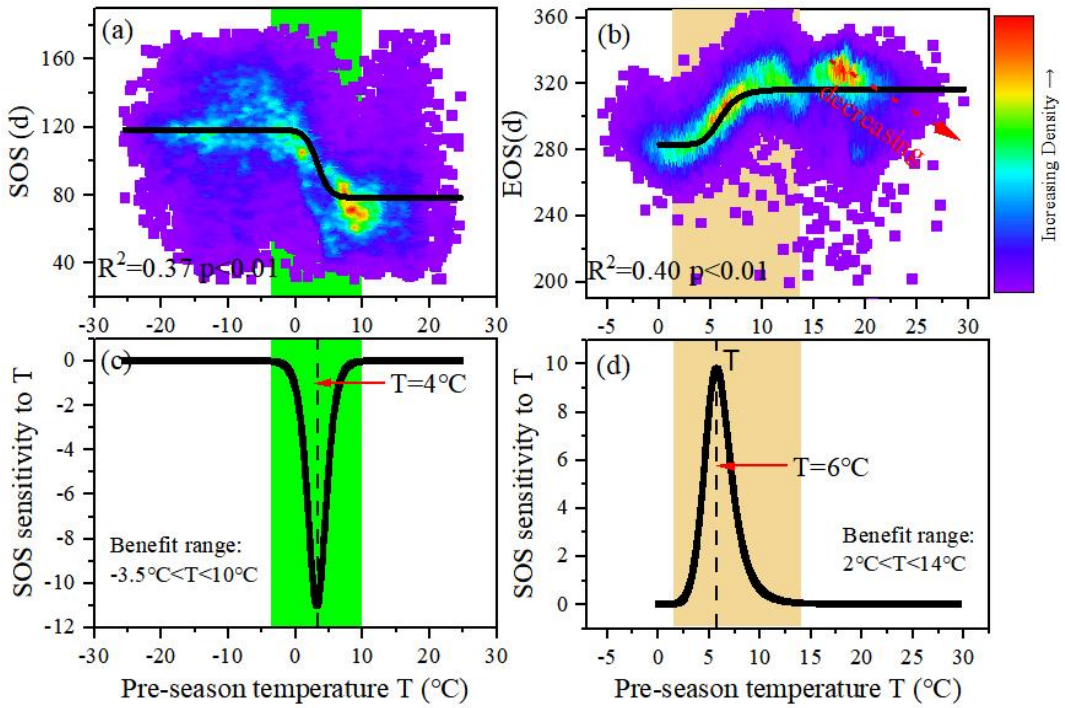

Figure 5. Relationships between pre-season temperature (T) and SOS/EOS (a,b), and the corresponding first-order derivatives with respect to temperature (c,d), representing phenological sensitivity to temperature.

To determine whether the temperature sensitivity influenced the logistic trends of phenology with LST, we conducted a nationwide fitting of phenology to T and derived logistic curves for SOS and EOS (Fig. 5). The first-order derivatives of the fitted curves, representing the phenological sensitivity to T, revealed warming benefits on SOS and EOS, ranging from -3.5 to 10 ℃ and 2.0 to 13.5 ℃, respectively. The highest sensitivity was observed at T = 4 ℃ for SOS and T = 6 ℃ for EOS. Notably, a decreasing trend for EOS was observed when T > 15 ℃, corresponding to the advanced EOS when T > 18.5 ℃ (Fig. 5d).

To assess the temperature sensitivity of phenological variations between urban and rural settings across vegetation types, we established regression models for Δ*SOS*, ΔEOS, and LST for each type (Fig. 6). Results showed that shrublands had the highest temperature sensitivity for both metrics, whereas CF displayed the lowest. The temperature response of MF and BF did not differ significantly.

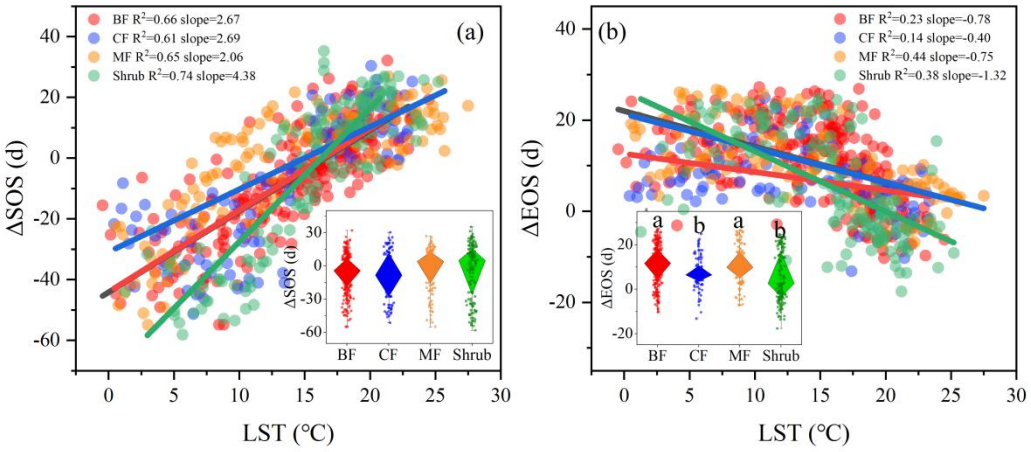

Figure 6. Relationships between LST and ΔSOS / ΔEOS across the 293 cities for four vegetation types. The inset subplots compare the mean phenological differences among vegetation groups. BF: Broad-leaf forest, CF: Coniferous forest, MF: Mixed forest, Shrubs: Shrublands.

3.3 Quantify the LST determined phenological sensitivity

To obtain LST-determined phenological sensitivity, the T in the first-order derivative curves shown in Figs. 5c and 5d was converted to LST based on the strong correlation between T and LST (Fig. S4). Three distinct LST thresholds were identified: phenological date stabilization thresholds, urban-rural disparity reversal thresholds, and phenological sensitivity saturation thresholds. Specifically, phenological date stabilization and urban-rural disparity reversal occur at LST = 12 ℃ (SOS) / 18.5 ℃ (EOS), while phenological sensitivity saturates at LST = 12.5 ℃ (SOS) / 4 ℃ (EOS). Based on the first-order derivatives, we identified the specific thresholds for phenological sensitivity. We observed that when background LST exceeded 12.5 ℃ for spring and 4 ℃ for autumn, the temperature sensitivity (Rt) began to significantly weaken. This indicates a saturation of the physiological response rate, even though the absolute urban-rural difference (ΔSOS/ΔEOS) might still persist until higher temperatures are reached.

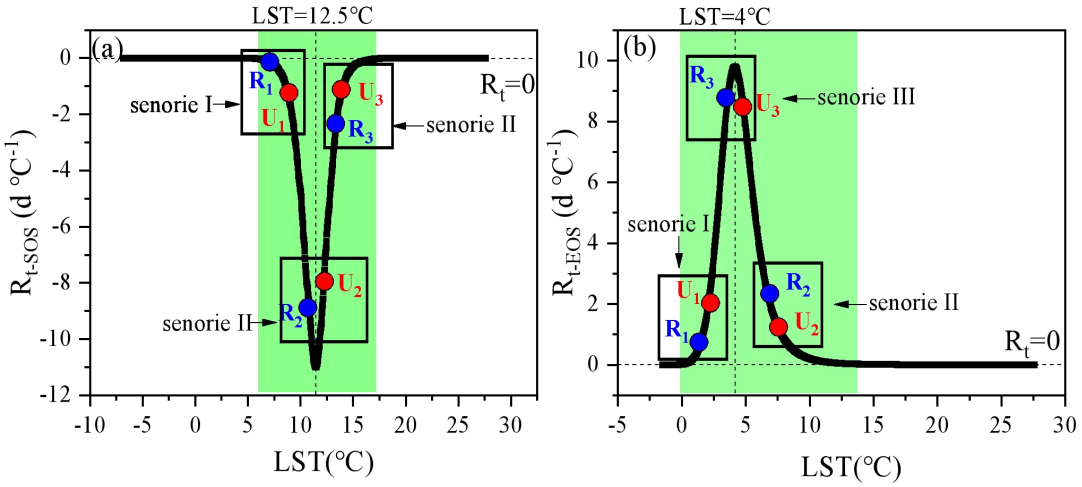

Figure 7. Schematic diagram of the three scenarios that likely occurred in urban (red dots) and rural (blue dots) regions for SOS (I: $LST_{R1} < LST_{U1} < 12.5$ ℃; II: 12.5 ℃ < $LST_{R2} < LST_{U2}$; III: $LST_{R3} < 12.5$ ℃ < LST_{U3}) and EOS (I: $LST_{R1} < LST_{U1} < 4$ ℃; II: 4 ℃ < $LST_{R2} < LST_{U2}$; III: $LST_{R3} < 4$ ℃ < LST_{U3}).

Scenario I: when LST was less than 12.5 ℃ (4 ℃) for SOS (EOS), higher LST was associated with heightened temperature sensitivity, resulting in urban regions (U_1) exhibiting higher sensitivity than rural regions (R_1) (Fig. 5).

Scenario II: when LST exceeded 12.5 ℃ (4 ℃) for SOS (EOS), temperature sensitivity weakened as LST increased, yet urban regions (U_2) still exhibited higher sensitivity than rural regions (R_2) (Fig. 5).

Scenario III: when urban LST surpassed 12.5 ℃ (4 ℃) while rural LST remained below 12.5 ℃ (4 ℃), the difference in sensitivity between urban and rural regions was inconclusive.

3.4 Phenology response to aridity

When the phenological responses were fitted to AI, $R_{t\text{-}SOS}$ and ΔSOS were positively related to AI (Fig. 8). When AI < 1.7, there was a decrease in absolute $R_{t\text{-}SOS}$ with increasing AI, indicating that increasing aridity weakened the temperature sensitivity of SOS. In contrast, when AI > 1.7, most urban areas exhibited positive $R_{t\text{-}SOS}$ (resulting in delayed SOS), with higher AI values corresponding to greater $R_{t\text{-}SOS}$, suggesting that severe drought conditions adversely delayed the onset of SOS.

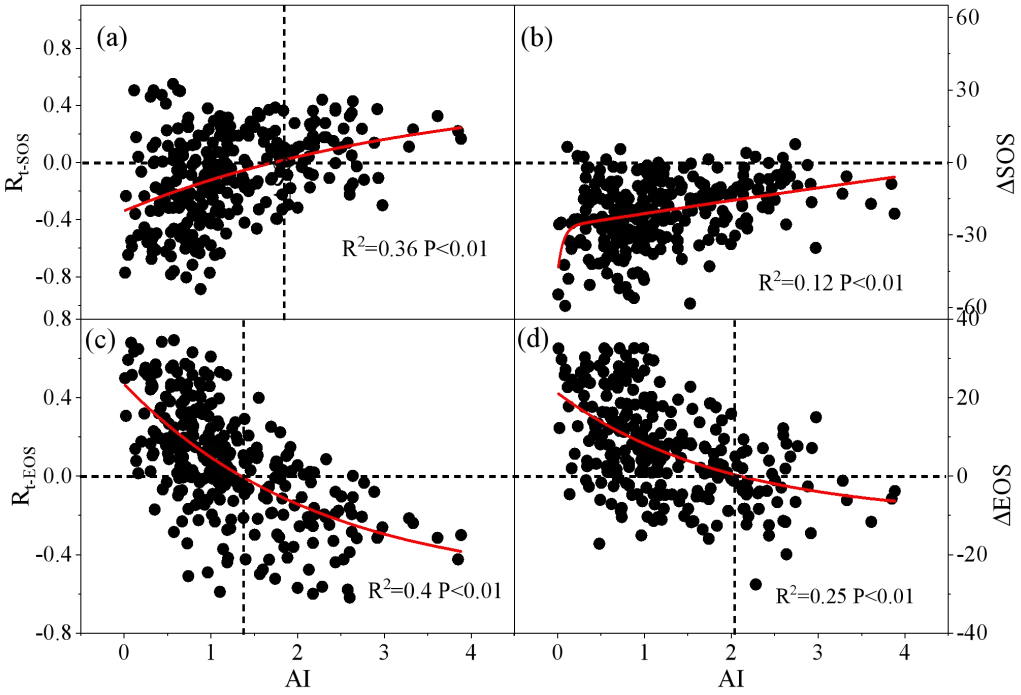

Figure 8. Phenological temperature sensitivity and urban-rural phenological differences determined by the aridity index (AI). When the phenological responses were fitted to AI, $R_{t\text{-}SOS}$ and ΔSOS were positively related to AI.

When $R_{t\text{-}EOS}$ and ΔEOS were fitted to AI, a negative relationship was observed. For $R_{t\text{-}EOS}$, when AI < 1.4, most $R_{t\text{-}EOS}$ values were positive, and decreased with AI, i.e., enhanced drought offset the benefit of urban warming on the delayed EOS. When AI > 1.4, most cities exhibited negative $R_{t\text{-}EOS}$, and higher AI values corresponded to more negative $R_{t\text{-}EOS}$. That is, extreme drought leads to passive warming effects on EOS. Notably, negative ΔEOS tended to appear when AI > 2.

AI was observed to advance ΔSOS and hasten ΔEOS across 293 cities, with this pattern holding true for all four vegetation types (Fig. 9). Notably, ΔSOS for CF showed less sensitivity to AI than the other vegetation types. Both BF and MF demonstrated lower sensitivities to AI for both ΔSOS and ΔEOS than shrublands.

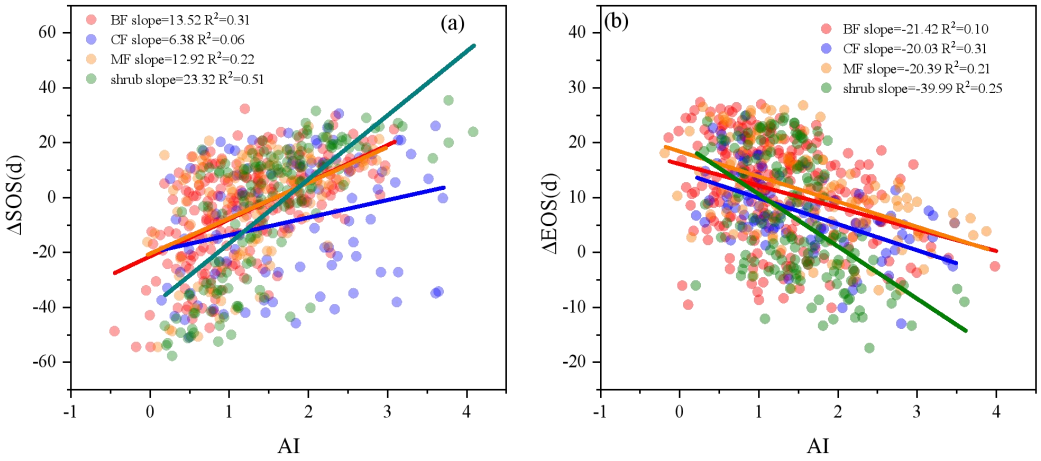

Figure 9. Relationships between AI and urban-rural phenological differences (ΔSOS, ΔEOS) across different vegetation types.

Panel (a): Scatter plot of ΔSOS versus AI with linear regression fits for each vegetation type.

Panel (b): Scatter plot of ΔEOS versus AI with linear regression fits for each vegetation type.

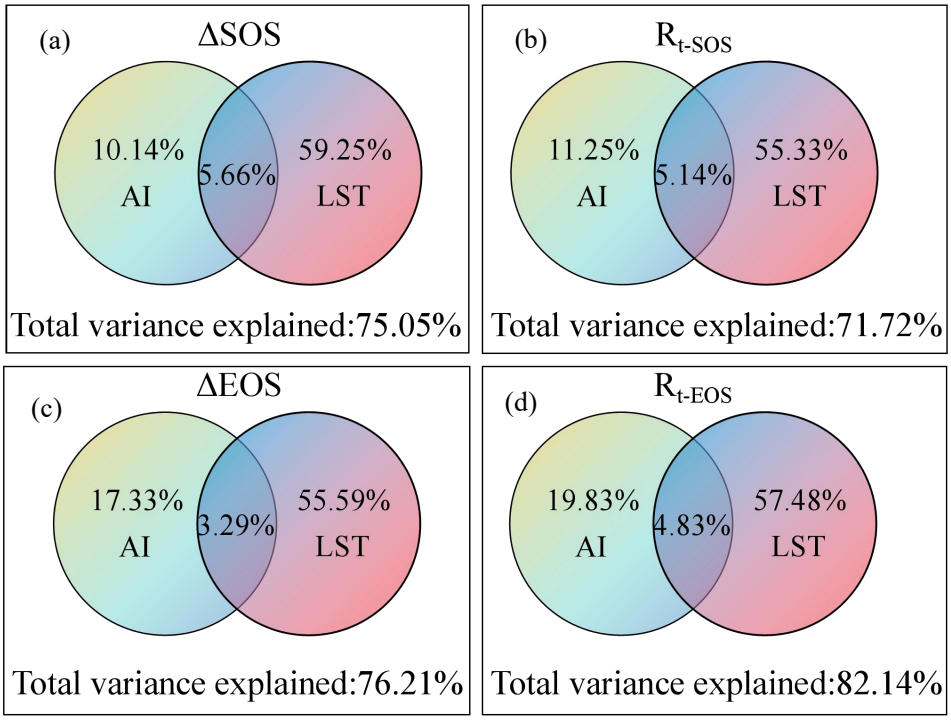

Figure 10. Venn diagrams illustrating the relative contributions of AI and LST to ΔSOS, ΔEOS, $R_{t\text{-}SOS}$, and $R_{t\text{-}EOS}$ across 293 Chinese cities. Note: Values in each section represent the percentage of variance independently explained by AI or LST

and their shared explanatory power in the overlapping region, and the total variance explained by both factors is labeled below each panel.

To further quantify the individual and combined contributions of LST and AI to phenological variations, a variance decomposition analysis was conducted (Legendre and Legendre, 2012; Fig. 10). The Venn diagram revealed that AI and LST explained 75.05%, 76.21%, 71.72% and 82.14% of the variance in ΔSOS, ΔEOS, $R_{t\text{-}SOS}$, and $R_{t\text{-}EOS}$, respectively (Fig. 10), and LST always contributed more to these phenological indicators. Additionally, the interaction effect of LST and AI ranged from 3.29% to 5.66%.

4. Discussion

4.1 Overall urbanization effects on plant phenology in China

Our multi-city assessment confirms a predominant urban-rural phenological divergence across China, characterized by advanced SOS and delayed EOS within a concentrated 10 km urbanization footprint. This consistent spatial pattern validates that urban warming acts as a primary driver of phenological shifts. Beyond mere thermal forcing, this convergence across 293 cities reflects the profound impact of urban microclimates on plant life cycles. The observed 10 km threshold is particularly significant as it suggests a localized but intense ecological footprint that necessitates specialized urban greening management strategies, especially in high-density northern cities where these shifts are most pronounced.

Spatially, the pronounced north-south gradient in ΔSOS and ΔEOS across China, as shown in Fig. 2, closely mirrors the spatial pattern of LST, reflecting stronger temperature sensitivity of vegetation phenology in northern regions than in the south. This finding aligns with previous research documenting greater phenological shifts in northern areas (Jia et al., 2021; Yang et al., 2025), and further highlights that background climate acts as a key modulator of urban phenological impacts. The more pronounced urban warming effects observed in coastal provinces relative to inland

cities (Fig. 2) likely stem from the buffering effect of the maritime climate on seasonal temperature constraints, which interacts with urban heat islands to amplify urban-rural phenological divergence. Moreover, the strong correlations between ΔSOS/ΔEOS, temperature sensitivity indicators ($R_{t\text{-}SOS}$ and $R_{t\text{-}EOS}$), LST, and AI, as presented in Fig. 3, confirm that background temperature and aridity are critical drivers shaping the magnitude of urbanization-induced phenological shifts across the 293 cities, rather than just passive correlates, validating the core hypothesis of this study.

Notably, the pattern of urban warming's benefit on vegetation phenology was consistent among the four vegetation types (Fig. S2). This consistency could be attributed to the ecological convergence of plants coexisting in shared local habitats within each city (Wang et al., 2016). Ecologically, the consistent 10 km effective footprint validates that urban environments function as distinct microclimatic islands. This spatial boundary conceptually highlights that urban ecological engineering and greening strategies must account for highly localized, rather than regional, thermal forcings.

4.2 Background temperature related phenological response variance

When we quantified phenological responses to temperature across the climatic gradient, clear logistic trends were observed for both SOS and EOS (Fig. 5). Consistent with this logistic trajectory, we observed that in urban areas, the growth rate for SOS/EOS began to plateau when temperatures exceeded 4 ℃/6 ℃, respectively (Fig. 5). Given the significant correlation between LST and T (Fig. S4), we anticipated a diminished sensitivity in phenology with higher LST (Fig. 7). These findings lend credibility to the "saturation" effect hypothesis, suggesting that the accelerating influence of warmth on vegetation phenology reported in earlier studies has its limits (Badeck et al., 2004; Li et al., 2021). Indeed, plants in southern regions exhibit not just a dampened phenological response but also a decelerated growth rate when faced with increasing temperatures (Li et al., 2021; Büntgen et al., 2019). As

illustrated by the first-order derivatives in Figs. 5c and 5d, the phenological sensitivity to temperature does not increase linearly, but peaks at T = 4 ℃ for SOS and T = 6 ℃ for EOS before rapidly declining. Specifically, the stabilization of urban SOS at 101.3 days and rural SOS at 129.7 days when LST was low (Fig. 4a) further demonstrated that plants reach a required physiological threshold that cannot be bypassed by additional thermal forcing. Collectively, these results highlight that threshold-based non-linear models rather than simple linear relationships are more suitable for predicting phenological responses under scenarios of continuous environmental warming, especially in urban settings. Conceptually, these saturation thresholds challenge the traditional linear paradigm of "warming-driven phenological advancement". By identifying explicit thermal boundaries, our framework establishes that the physiological capacity of urban vegetation to capitalize on UHI warming is strictly finite.

The observation of temperature saturation for the SOS in our study likely stems from the chilling requirements for vernalization (Kim et al., 2009; Hanninen et al., 2019). Typically, vegetation needs to undergo a period of exposure to low chilling temperatures to break dormancy. This mechanism is consistent with our spatial observations in Fig. 2a, where cities in lower latitudes (warmer regions) exhibited significantly smaller ΔSOS values. This suggests that in these warmer regions, the higher background LST may fail to satisfy the necessary chilling requirements, leading to the diminished phenological sensitivity we quantified in Fig. 3. Moreover, an earlier onset of greening increases the risk of damage from freezing events, posing a survival threat to plants (Duan et al., 2011; Wang et al., 2015). This phenomenon explains the delayed SOS in approximately 16% of the cities under study, mainly distributed in low-latitude regions (Fig. 4).

Regarding the EOS, a moderate increase in temperature can enhance the activity of photosynthetic enzymes (Shi et al., 2014), slow down the degradation of chlorophyll (Fracheboud et al., 2009), reduce the risk of frost exposure in autumn, and increase the potential for growth and photosynthetic production, ultimately promoting the extension of the growing season. However, the benefits of increased temperature

can be offset by the negative impacts of heat waves and excessive thermal stress (Mathur et al., 2014). Our data in Figs. 5b and 5d provide direct evidence for this: when pre-season temperature (T) exceeded 15 ℃, a decreasing trend for EOS was observed. This aligns with the intersection points identified in Figs. 4c and 4d at LST = 18 ℃, where the urban-rural phenology difference reverses, confirming that excessive heat in urban centers triggers premature leaf senescence rather than further delaying it. In fact, when T > 15 ℃, EOS tends to be reduced, with an increased sensitivity to temperature changes (Estiarte and Peñuelas, 2015; Fig. 5b).

Despite the existence of "saturation" effects, lower background temperatures do not necessarily correspond to higher phenological sensitivity (Fig. 4b, c). For SOS, when T < 4 ℃, the phenological sensitivity approached zero with decreased T (Fig. 4c), which led to a stable SOS of 120 days (Fig. 5a,c). In fact, phenological events such as bud burst could not be triggered when the threshold for high forcing temperatures was not reached (Hanninen et al., 2019). For EOS, when T > 6 ℃, the increased T sensitivity produces more EOS advancement in warmer regions. This reversal may be associated with abscisic acid synthesis induced by low temperatures, which accelerates the progress of defoliation.

Beyond thermal controls alone, our findings regarding the aridity-driven modulation of phenological responses provide a critical geographic context that complements previous observations. While earlier studies primarily emphasized thermal forcing as the dominant driver of urban phenology (Meng et al., 2020), our results demonstrate that AI acts as a significant "environmental filter" that can override or even reverse warming benefits. As shown in Figs. 8 and 10, the high explanatory power of AI (17.33% for ΔEOS) suggests that in water-limited regions of northern and western China, the physiological stress induced by drought prevents plants from utilizing the additional heat provided by the Urban Heat Island (UHI) effect. This phenomenon is consistent with the "resource limitation" theory, where plant development is constrained by the most limiting resource (water; Harpole et al., 2011), regardless of optimal temperatures. Compared to coastal cities where water is abundant, the weakened warming benefits in arid inland cities highlight the need for

607 regionally differentiated urban irrigation strategies to maintain ecological productivity.
608 However, when LST < 12.5 ℃, warming regions exhibited higher urban-rural
609 differences in $\Delta R_{t\text{-}SOS}$, which contradicted the weakened urban-rural difference in
610 $\Delta R_{t\text{-}SOS}$ reported in the previous study. For EOS, the warming benefits only occurred
611 when 0 < LST < 18 ℃. Moreover, the weakened sensitivity was only detected in the
612 LST interval of LST > 4 ℃. The conclusions of weakened $\Delta R_{t\text{-}SOS}$ and $\Delta R_{t\text{-}EOS}$ in the
613 USA may reflect that their LST ranges were mostly within the range of 8 ℃ to 22 ℃.

614 4.3 AI related phenological response variance

615 In addition to background temperature (LST), the aridity index (AI) drives
616 significant spatial variation in urban-rural phenological disparities (ΔSOS, ΔEOS).
617 Spatially, the coastal cities experienced more benefits from urban warming (Fig. 2).
618 Our statistical decomposition in Fig. 10 further elucidates this aridity-driven
619 modulation, showing that AI and LST together explain more than 75% of the variance
620 in ΔSOS and ΔEOS. Notably, the fact that AI explains 17.33% of the variation in
621 ΔEOS (Fig. 10c) supports our inference that water availability is a critical limiting
622 factor in autumn. This is further substantiated by the positive correlation between
623 ΔSOS and AI in Fig. 8b, which quantifies how increasing aridity progressively offsets
624 the advanced green-up typically induced by urban warming. These results highlight
625 that the warming benefits on vegetation phenology will be weakened in those
626 drought-dominated regions. In fact, the delayed SOS has already been demonstrated
627 in previous studies (Ji et al., 2021; Yu et al., 2003).

628 Water deficit inhibits leaf growth via chemical signals (Knauer et al., 2017), and
629 urbanization exacerbates drought stress (Zhang et al., 2019; Pollastrini et al., 2019),
630 further weakening or even reversing the positive effects of urban warming on
631 phenology. Furthermore, in water-stressed regions, temperatures are already close to
632 the optimum for photosynthesis, thus fewer benefits are expected (Peñuelas et al.,
633 2004). The weakened temperature sensitivity in drought-prone cities is likely to lead
634 to less extension of the growing season.

Notably, the influence of AI on autumn phenology response was higher than that on spring phenology response (Fig. 10). During spring leaf development, plants may use water stored in their bodies to support the growth of new leaves (Shi et al., 2023). Supporting evidence comes from the synchrony between plant water storage and leaf sprouting for the boreal and temperate forests (Tian et al., 2018). In this case, plants may have relatively little demand for external water supply, especially in some wetter areas. By comparison, in summer and autumn, plant transpiration is higher, and water demand is greater (Wu et al., 2022), so the influence of drought severity on plant phenology is more pronounced. The overarching ecological implication here is a profound vulnerability: as background climates dry under global change, the compounding stress of UHI and background aridity may lead to "phenological compression". In arid urban ecosystems, this moisture deficit effectively neutralizes the anticipated carbon sequestration benefits of thermally extended growing seasons, rendering them highly sensitive to future climate extremes.

4.4 Phenological response variation among different vegetation types

The phenological response to LST and AI varies significantly across vegetation types, reflecting the influence of distinct ecological strategies. Our results (Figs. 6 and 9) demonstrate that shrublands are the most sensitive to both warming and aridity, likely due to their opportunistic resource utilization strategy and higher leaf turnover rates (Xiong et al., 2024). In contrast, coniferous forests exhibited a muted response to both drivers (Malla et al., 2023). While our analysis relies on broad land-cover categories and does not directly measure species-specific functional traits, these discrepancies likely reflect generalized divergent ecological strategies among the vegetation groups.

This insensitivity is substantiated by our AI-sensitivity analysis (Fig. 9a), suggesting that the conservative hydraulic traits of conifers — such as needle morphology and lower stomatal conductance (Sperry et al., 2002; Brodribb and McAdam, 2013) — act as a buffer against the "aridity-driven inhibition" that more

severely affects broadleaf species. Based on generalized ecological principles, this might be associated with typical drought-resistant adaptations found in many conifers (e.g., needle morphology and stricter stomatal control), which could limit the potential positive impact of warming on their phenology. In contrast, the heightened sensitivity of shrublands observed in our dataset aligns with literature suggesting more opportunistic resource utilization strategies in shrubs (Xiong et al., 2024).

By considering these functional differences, our study provides a more nuanced understanding of urban ecosystem resilience, suggesting that urban greening programs should prioritize drought-resistant coniferous or mixed forest structures in regions where the warming-saturation effect is most pronounced. However, we note that these functional interpretations remain broad generalizations; future studies incorporating field-based, species-level trait measurements are required to mechanistically validate these large-scale categorical patterns. Recognizing these trait-mediated responses is a crucial conceptual step for urban forestry. It indicates that building climate-resilient urban ecosystems requires shifting from generic greening to deploying specific functional traits—such as the conservative hydraulic strategies of conifers—to buffer against the coupled heat-aridity saturation effects.

5. Conclusion

Our study used remote sensing data to investigate the impact of urbanization on vegetation phenology across 293 Chinese cities for 2010 to 2020. Urban heat islands consistently advanced the start of the growing season (SOS) by 12.06 days and delayed the end of the growing season (EOS) by 9.86 days relative to rural areas. However, the magnitude of these shifts varied markedly with background land surface temperature (LST) and aridity index (AI), indicating that urban warming benefits are not universally distributed but are constrained by local climatic context.

We identified a non-linear saturation effect in phenological sensitivity to urban warming. Temperature sensitivity peaked at 4 ℃ (spring) and 6 ℃ (autumn), and weakened significantly beyond saturation thresholds of 12.5 ℃ for SOS and 4 ℃ for

EOS. Within the effective ranges of 3.5 to 17.5 ℃ (SOS) and 0–18 ℃ (EOS), urban warming exerted pronounced positive effects on phenological shifts; outside these ranges, sensitivity approached zero. Notably, extreme high temperatures reversed the beneficial effects for EOS, causing weakly delayed or even advanced senescence in warm urban regions.

Aridity emerged as a critical negative regulator of warming benefits. Across most AI ranges, increasing aridity attenuated the positive effects of UHI on both SOS and EOS. Within the intermediate aridity band of $1.4 < AI < 2.0$, warming benefits were entirely reversed. Consequently, coastal cities with lower AI exhibited substantially larger urban-rural phenological disparities than arid inland cities, where coupled heat-aridity stress compressed the effective growing season.

Collectively, these findings challenge the linear assumption that urban warming universally extends the growing season. Instead, they demonstrate that phenological responses to UHI are bounded by finite physiological limits and modulated by water availability. For urban ecological planning, our results imply that greening strategies must be climate-specific: drought-resistant vegetation structures should be prioritized in arid regions where saturation occurs at lower thermal thresholds, whereas coastal and northern cities can more effectively harness UHI benefits for growing season extension. Future research incorporating species-level functional traits and process-based phenology models will be essential to refine these thresholds and project urban ecosystem dynamics under continued global warming.

Data availability statement

The data that support the findings of this study are available in those public domain resources that listed in the table 1.

Author contributions

Lin Xingwen: Conceptualization, Methodology, Funding Acquisition;

Zhang Zhenzhen: Data curation, Writing - Original draft preparation;

Hu Xinxin: Methodology, Formal analysis, Validation, Writing - review and editing;
Zhang Yongqi: Visualization, Investigation;
Sun Liheng, Wu Chaofan and Cui Shufen: Supervision;
Zhang Zhaoyang, Chen Yuanjian: Software, Validation;
Wen Qingqing: Funding Acquisition.

Competing interests

The authors declared that the research was conducted in the absence of any commercial or financial relationships that could be construed as a potential conflict of interest.

Acknowledgements

We appreciate the valuable suggestions from the Associate and anonymous reviewers, which substantially improved this manuscript. We also acknowledge the computing support provided by our university and the members of our research group for their assistance throughout this work.

Funding

This study was supported by “Jinhua scientific and technological projects (grant number, 2026-3-108, 2024-3-002), Open Research Project of Innovation Center of Yangtze River Delta, Zhejiang University (grant number: 2025KFKY004)”.

References

Angilletta, M. J.: Thermal Adaptation: A Theoretical and Empirical Synthesis, Oxford University Press, Oxford, https://doi.org/10.1093/acprof:oso/9780198570875.001.1, 2009.

Badeck, F.-W., Bondeau, A., Böttcher, K., Doktor, D., Lucht, W., Schaber, J., and Sitch, S.: Responses of spring phenology to climate change, New Phytol., 162, 295–309,

https://doi.org/10.1111/j.1469-8137.2004.01059.x, 2004.

Brodribb, T. J. and McAdam, S. A. M.: Abscisic acid mediates a divergence in the drought response of two conifers, Plant Physiol., 162, 1370–1377, https://doi.org/10.1104/pp.113.217877, 2013.

Buyantuyev, A. and Wu, J.: Urbanization diversifies land surface phenology in arid environments: Interactions among vegetation, climatic variation, and land use pattern in the Phoenix metropolitan region, USA, Landsc. Urban Plan., 105, 149–159, https://doi.org/10.1016/j.landurbplan.2011.12.013, 2012.

Büntgen, U., Krusic, P. J., Piermattei, A., Coomes, D. A., Esper, J., Myglan, V. S., Kirdyanov, A. V., Camarero, J. J., Crivellaro, A., and Körner, C.: Limited capacity of tree growth to mitigate the global greenhouse effect under predicted warming, Nat. Commun., 10, 2171, https://doi.org/10.1038/s41467-019-10174-4, 2019.

Cai, Z., Jönsson, P., Jin, H., and Eklundh, L.: Performance of smoothing methods for reconstructing NDVI time-Series and estimating vegetation phenology from MODIS Data, Remote Sens., 9, 1271, https://doi.org/10.3390/rs9121271, 2017.

Čehulić, I., Sever, K., Katičić Bogdan, I., Jazbec, A., Škvorc, Ž., and Bogdan, S.: Drought Impact on Leaf Phenology and Spring Frost Susceptibility in a Quercus robur L. Provenance Trial, Forests, 10, 50, https://doi.org/10.3390/f10010050, 2019.

Chmielewski, F.-M. and Rötzer, T.: Response of tree phenology to climate change across Europe, Agric. For. Meteorol., 108, 101–112, https://doi.org/10.1016/S0168-1923(01)00233-7, 2001.

Cong, N., Piao, S., Chen, A., Wang, X., Lin, X., Chen, S., Han, S., Zhou, G., and Zhang, X.: Spring vegetation green-up date in China inferred from SPOT NDVI data: A multiple model analysis, Agr. Forest Meteorol., 165, 104–113, https://doi.org/10.1016/j.agrformet.2012.06.009, 2012.

Dallimer, M., Tang, Z., Gaston, K. J., and Davies, Z. G.: The extent of shifts in vegetation phenology between rural and urban areas within a human-dominated region, Ecol. Evol., 6, 1942–1953, https://doi.org/10.1002/ece3.1990, 2016.

Ding, H., Xu, L., Elmore, A. J., Ma, X., and Li, X.: Vegetation phenology influenced by rapid urbanization of The Yangtze Delta region, Remote Sens., 12, 1783,

https://doi.org/10.3390/rs12111783, 2020.

Doncaster, C. P.: Structural Equation Modeling and Natural Systems, Fish Fish., 8, 368–369, https://doi.org/10.1111/j.1467-2979.2007.00260.x, 2007.

Duan, J., Zhang, Q.-B., Lv, L., and Zhang, C.: Regional-scale winter-spring temperature variability and chilling damage dynamics over the past two centuries in southeastern China, Clim. Dynam., 39, 919–928, https://doi.org/10.1007/s00382-011-1323-9, 2011.

Elvidge, C. D., Baugh, K., Zhizhin, M., Hsu, F. C., and Ghosh, T.: VIIRS night-time lights, Int. J. Remote Sens., 38, 5860–5879, https://doi.org/10.1080/01431161.2017.1342050, 2017.

Estiarte, M. and Peñuelas, J.: Alteration of the phenology of leaf senescence and fall in winter deciduous species by climate change: effects on nutrient proficiency, Glob. Change Biol., 21, 1005–1017, https://doi.org/10.1111/gcb.12804, 2015.

Fan, J., He, H., Hu, T., Zhang, P., Yu, X., and Zhou, Y.: Estimation of landscape pattern changes in BRICS from 1992 to 2013 using DMSP-OLS NTL images, J. Indian Soc. Remote Sens., 47, 725–735, https://doi.org/10.1007/s12524-019-00963-1, 2019.

Fracheboud, Y., Luquez, V., Bjorken, L., Sjodin, A., Tuominen, H., and Jansson, S.: The control of autumn senescence in European aspen, Plant Physiol., 149, 1982–1991, https://doi.org/10.1104/pp.108.133249, 2009.

Gazal, R., White, M. A., Gillies, R., Rodemaker, E. L. I., Sparrow, E., and Gordon, L.: GLOBE students, teachers, and scientists demonstrate variable differences between urban and rural leaf phenology, Glob. Change Biol., 14, 1568–1580, https://doi.org/10.1111/j.1365-2486.2008.01602.x, 2008.

Ge, W., Han, J., Zhang, D., and Wang, F.: Divergent impacts of droughts on vegetation phenology and productivity in the Yungui Plateau, southwest China, Ecol. Indic., 127, 107743, https://doi.org/10.1016/j.ecolind.2021.107743, 2021.

Gow, L. J., Barrett, D. J., Renzullo, L. J., Phinn, S. R., and O'Grady, A. P.: Characterising groundwater use by vegetation using a surface energy balance model and satellite observations of land surface temperature, Environ. Modell. Softw., 80, 66–82, https://doi.org/10.1016/j.envsoft.2016.02.021, 2016.

Grimm, N. B., Faeth, S. H., Golubiewski, N. E., Redman, C. L., Wu, J., Bai, X., and Briggs, J. M.: Global change and the ecology of cities, Science, 319, 756–760, https://doi.org/10.1126/science.1150195, 2008.

Hanninen, H., Kramer, K., Tanino, K., Zhang, R., Wu, J., and Fu, Y. H.: Experiments are necessary in process-based tree phenology modelling, Trends Plant Sci., 24, 199–209, https://doi.org/10.1016/j.tplants.2018.11.006, 2019.

Harpole, W. S., Ngai, J. T., Cleland, E. E., Seabloom, E. W., Borer, E. T., Bracken, M. E., Elser, J. J., Gruner, D. S., Hillebrand, H., Shurin, J. B., and Smith, J. E.: Nutrient co-limitation of primary producer communities, Ecol. Lett., 14, 852–862, https://doi.org/10.1111/j.1461-0248.2011.01651.x, 2011.

He, C., Gao, B., Huang, Q., Ma, Q., and Dou, Y.: Environmental degradation in the urban areas of China: Evidence from multi-source remote sensing data, Remote Sens. Environ., 193, 65–75, https://doi.org/10.1016/j.rse.2017.02.027, 2017.

Jeong, S.-J., Park, H., Ho, C.-H., and Kim, J.: Impact of urbanization on spring and autumn phenology of deciduous trees in the Seoul Capital Area, South Korea, Int. J. Biometeorol., 63, 627–637, https://doi.org/10.1007/s00484-018-1610-7, 2019.

Ji, S., Ren, S., Li, Y., Dong, J., Wang, L., Quan, Q., and Liu, J.: Diverse responses of spring phenology to preseason drought and warming under different biomes in the North China Plain, Sci. Total Environ., 766, 144437, https://doi.org/10.1016/j.scitotenv.2020.144437, 2021.

Jia, W., Zhao, S., Zhang, X., Liu, S., Henebry, G. M., and Liu, L.: Urbanization imprint on land surface phenology: The urban-rural gradient analysis for Chinese cities, Glob. Change Biol., 27, 2895–2904, https://doi.org/10.1111/gcb.15602, 2021.

Jönsson, P. and Eklundh, L.: TIMESAT—a program for analyzing time-series of satellite sensor data, Comput. Geosci., 30, 833 – 845, https://doi.org/10.1016/j.cageo.2004.05.006, 2004.

Kang, X., Hao, Y., Cui, X., Chen, H., Huang, S., Du, Y., Li, W., Kardol, P., Xiao, X., and Cui, L.: Variability and changes in climate, phenology, and gross primary production of an Alpine wetland ecosystem, Remote Sens., 8, 391, https://doi.org/10.3390/rs8050391, 2016.

Ketola, T. and Kristensen, T. N.: Experimental approaches for testing if tolerance curves are useful for predicting fitness in fluctuating environments, Front. Ecol. Evol., 5, 129, https://doi.org/10.3389/fevo.2017.00129, 2017.

Kim, D. H., Doyle, M. R., Sung, S., and Amasino, R. M.: Vernalization: winter and the timing of flowering in plants, Annu. Rev. Cell Dev. Biol., 25, 277–299, https://doi.org/10.1146/annurev.cellbio.042308.113411, 2009.

Knauer, J., Zaehle, S., Reichstein, M., Medlyn, B. E., Forkel, M., Hagemann, S., and Werner, C.: The response of ecosystem water-use efficiency to rising atmospheric CO2 concentrations: sensitivity and large-scale biogeochemical implications, New Phytol., 213, 1654–1666, https://doi.org/10.1111/nph.14288, 2017.

Legendre, P. and Legendre, L.: Numerical Ecology, 3rd ed., Elsevier, Amsterdam, ISBN 978-0-444-53869-7, 2012.

Li, K., Wang, C., Sun, Q., Rong, G., Tong, Z., Liu, X., and Zhang, J.: Spring phenological sensitivity to climate Change in the northern hemisphere: comprehensive evaluation and driving force analysis, Remote Sens., 13, 1972, https://doi.org/10.3390/rs13101972, 2021.

Malla, R., Neupane, P. R., and Köhl, M.: Climate change impacts: Vegetation shift of broad-leaved and coniferous forests, Trees For. People, 14, 100457, https://doi.org/10.1016/j.tfp.2023.100457, 2023.

Mathur, S., Agrawal, D., and Jajoo, A.: Photosynthesis: response to high temperature stress, J. Photochem. Photobiol. B, 137, 116–126, https://doi.org/10.1016/j.jphotobiol.2014.01.010, 2014.

Meng, L., Mao, J., Zhou, Y., Richardson, A. D., Lee, X., Thornton, P. E., Ricciuto, D. M., Li, X., Dai, Y., Shi, X., and Jia, G.: Urban warming advances spring phenology but reduces the response of phenology to temperature in the conterminous United States, Proc. Natl. Acad. Sci. USA, 117, 4228–4233, https://doi.org/10.1073/pnas.1911117117, 2020.

Mu, Q., Zhao, M., and Running, S. W.: Improvements to a MODIS global terrestrial evapotranspiration algorithm, Remote Sens. Environ., 115, 1781 – 1800, https://doi.org/10.1016/j.rse.2011.02.019, 2011.

862 Pablos, M., Martínez-Fernández, J., Piles, M., Sánchez, N., Vall-llossera, M., and Camps,
863 A.: Multi-temporal evaluation of soil moisture and land surface temperature
864 dynamics using in situ and satellite observations, Remote Sens., 8, 587,
865 https://doi.org/10.3390/rs8070587, 2016.
866 Peng, S.: 1-km monthly precipitation dataset for China (1901-2021), National Tibetan
867 Plateau / Third Pole Environment Data Center [data set],
868 https://doi.org/10.5281/zenodo.3185722, 2020.
869 Peng, J., Wu, C., Zhang, X., Wang, X., and Gonsamo, A.: Satellite detection of cumulative
870 and lagged effects of drought on autumn leaf senescence over the Northern
871 Hemisphere, Glob. Change Biol., 25, 2174–2188, https://doi.org/10.1111/gcb.14627,
872 2019.
873 Peñuelas, J., Gordon, C., Llorens, L., Nielsen, T., Tietema, A., Beier, C., Bruna, P.,
874 Emmett, B., Estiarte, M., and Gorissen, A.: Nonintrusive field experiments show
875 different plant responses to warming and drought among sites, seasons, and species
876 in a north-south European gradient, Ecosystems, 7, 598–612,
877 https://doi.org/10.1007/s10021-004-0179-7, 2004.
878 Piao, S., Fang, J., Zhou, L., Ciais, P., and Zhu, B.: Variations in satellite-derived
879 phenology in China's temperate vegetation, Glob. Change Biol., 12, 672–685,
880 https://doi.org/10.1111/j.1365-2486.2006.01123.x, 2006.
881 Pinheiro, J. C. and Bates, D. M.: Mixed-Effects Models in S and S-PLUS, Springer, New
882 York, ISBN 978-0-387-22747-4, https://doi.org/10.1007/b98882, 2000.
883 Pollastrini, M., Puletti, N., Selvi, F., Iacopetti, G., and Bussotti, F.: Widespread crown
884 defoliation after a drought and heat wave in the forests of Tuscany (Central Italy) and
885 their recovery—A case study from summer 2017, Front. For. Glob. Change, 2, 74,
886 https://doi.org/10.3389/ffgc.2019.00074, 2019.
887 Qiao, Z., Tian, G., and Xiao, L.: Diurnal and seasonal impacts of urbanization on the
888 urban thermal environment: A case study of Beijing using MODIS data, ISPRS J.
889 Photogramm. Remote Sens., 85, 93–101,
890 https://doi.org/10.1016/j.isprsjprs.2013.08.010, 2013.
891 Qiu, T., Song, C., and Li, J.: Impacts of urbanization on vegetation phenology over the

past three decades in Shanghai, China, Remote Sens., 9, 970, https://doi.org/10.3390/rs9090970, 2017.

Rustad, L., Campbell, J., Marion, G., Norby, R., Mitchell, M., Hartley, A., Cornelissen, J., Gurevitch, J., and Gcte, N.: A meta-analysis of the response of soil respiration, net nitrogen mineralization, and aboveground plant growth to experimental ecosystem warming, Oecologia, 126, 543–562, https://doi.org/10.1007/s004420000544, 2001.

Sage, R. F. and Kubien, D. S.: The temperature response of C3 and C4 photosynthesis, Plant Cell Environ., 30, 1086–1106, https://doi.org/10.1111/j.1365-3040.2007.01682.x, 2007.

Shi, C., Sun, G., Zhang, H., Xiao, B., Ze, B., Zhang, N., and Wu, N.: Effects of warming on chlorophyll degradation and carbohydrate accumulation of Alpine herbaceous species during plant senescence on the Tibetan Plateau, PLoS One, 9, e107874, https://doi.org/10.1371/journal.pone.0107874, 2014.

Shi, W., Li, J., Zhan, H., Yu, L., Wang, C., and Wang, S.: Relation between water storage and photoassimilate accumulation of neosinocalamus affinis with phenology, Forests, 14, 531, https://doi.org/10.3390/f14030531, 2023.

Sperry, J. S., Hacke, U. G., Oren, R., and Comstock, J. P.: Water deficits and hydraulic limits to leaf water supply, Plant Cell Environ., 25, 251 – 263, https://doi.org/10.1046/j.0016-8025.2001.00799.x, 2002.

Tian, F., Wigneron, J.-P., Ciais, P., Chave, J., Ogée, J., Peñuelas, J., Ræbild, A., Domec, J.-C., Tong, X., Brandt, M., Mialon, A., Rodriguez-Fernandez, N., Tagesson, T., Al-Yaari, A., Kerr, Y., Chen, C., Myneni, R. B., Zhang, W., Ardö, J., and Fensholt, R.: Coupling of ecosystem-scale plant water storage and leaf phenology observed by satellite, Nat. Ecol. Evol., 2, 1428–1435, https://doi.org/10.1038/s41559-018-0630-3, 2018.

Wan, Z.: New refinements and validation of the MODIS Land-Surface Temperature/Emissivity products, Remote Sens. Environ., 112, 59–74, https://doi.org/10.1016/j.rse.2006.06.026, 2008.

Wang, C., Cao, R., Chen, J., Rao, Y., and Tang, Y.: Temperature sensitivity of spring vegetation phenology correlates to within-spring warming speed over the Northern

Hemisphere, Ecol. Indic., 50, 62–68, https://doi.org/10.1016/j.ecolind.2014.11.004, 2015.

Wang, C., Tang, Y., and Chen, J.: Plant phenological synchrony increases under rapid within-spring warming, Sci. Rep., 6, 25460, https://doi.org/10.1038/srep25460, 2016.

White, M. A., De Beurs, K. M., Didan, K., Inouye, D. W., Richardson, A. D., Jensen, O. P., O'Keefe, J., Zhang, G., Nemani, R. R., Van Leeuwen, W. J. D., Brown, J. F., De Wit, A., Schaepman, M., Lin, X., Dettinger, M., Bailey, A. S., Kimball, J., Schwartz, M. D., Baldocchi, D. D., Lee, J. T., and Lauenroth, W. K.: Intercomparison, interpretation, and assessment of spring phenology in North America estimated from remote sensing for 1982-2006, Glob. Change Biol., 15, 2335–2359, https://doi.org/10.1111/j.1365-2486.2009.01910.x, 2009.

Wu, C., Peng, J., Ciais, P., Peñuelas, J., Wang, H., Beguería, S., Black, T. A., Jassal, R. S., Zhang, X., Yuan, W., Liang, E., Wang, X., Hua, H., Liu, R., Ju, W., Fu, Y. H., and Ge, Q.: Increased drought effects on the phenology of autumn leaf senescence, Nat. Clim. Change, 12, 943–949, https://doi.org/10.1038/s41558-022-01464-9, 2022.

Xiong, X., Wu, H., Wei, X., and Jiang, M.: Contrasting temperature and light sensitivities of spring leaf phenology between understory shrubs and canopy trees: Implications for phenological escape, Agric. For. Meteorol., 355, 110144, https://doi.org/10.1016/j.agrformet.2024.110144, 2024.

Yang, H., Zhang, Q., Zhang, S., Wang, X., and Yu, H.: Joint control of urban expansion and climate change on urban-rural vegetation phenology gradient in 31 cities of China, Front. Ecol. Evol., 13, 1637210, https://doi.org/10.3389/fevo.2025.1637210, 2025.

Yao, R., Wang, L., Huang, X., Guo, X., Niu, Z., and Liu, H.: Investigation of Urbanization effects on land Surface phenology in Northeast China during 2001–2015, Remote Sens., 9, 66, https://doi.org/10.3390/rs9010066, 2017.

Yu, F., Price, K. P., Ellis, J., and Shi, P.: Response of seasonal vegetation development to climatic variations in eastern central Asia, Remote Sens. Environ., 87, 42–54, https://doi.org/10.1016/S0034-4257(03)00144-5, 2003.

Yuan, M., Zhao, L., Lin, A., Wang, L., Li, Q., She, D., and Qu, S.: Impacts of preseason

drought on vegetation spring phenology across the Northeast China Transect, Sci. Total Environ., 738, 140297, https://doi.org/10.1016/j.scitotenv.2020.140297, 2020.

Zhang, X., Friedl, M. A., Schaaf, C. B., Strahler, A. H., and Schneider, A.: The footprint of urban climates on vegetation phenology, Geophys. Res. Lett., 31, L12209, https://doi.org/10.1029/2004GL020137, 2004.

Zhang, X., Friedl, M. A., and Schaaf, C. B.: Global vegetation phenology from Moderate Resolution Imaging Spectro radiometer (MODIS): Evaluation of global patterns and comparison with in situ measurements, J. Geophys. Res.-Biogeo., 111, G04017, https://doi.org/10.1029/2006JG000217, 2006.

Zhang, X., Chen, N., Sheng, H., Ip, C., Yang, L., Chen, Y., Sang, Z., Tadesse, T., Lim, T. P. Y., Rajabifard, A., Bueti, C., Zeng, L., Wardlow, B., Wang, S., Tang, S., Xiong, Z., Li, D., and Niyogi, D.: Urban drought challenge to 2030 sustainable development goals, Sci. Total Environ., 693, 133536, https://doi.org/10.1016/j.scitotenv.2019.07.342, 2019.

Zheng, W., Liu, Y., Yang, X., and Fan, W.: Spatiotemporal variations of forest vegetation phenology and its response to climate change in northeast China, Remote Sens., 14, 2909, https://doi.org/10.3390/rs14122909, 2022.

Zhou, D., Zhao, S., Zhang, L., and Liu, S.: Remotely sensed assessment of urbanization effects on vegetation phenology in China's 32 major cities, Remote Sens. Environ., 176, 272–281, https://doi.org/10.1016/j.rse.2016.02.010, 2016.